Available online at www.sciencedirect.com

SciVerse ScienceDirect

Ceramics International 39 (2013) 1741–1747

CERAMICS INTERNATIONAL

www.elsevier.com/locate/ceramint

Carbon-doped Li_2SnO_3/graphene as an anode material for lithium-ion batteries

Yang Zhao, Ying Huang*, Qiufen Wang, Xiaoya Wang, Meng Zong

Department of Applied Chemistry, The Key Laboratory of Space Applied Physics and Chemistry, Ministry of Education, School of Science, Northwestern Polytechnical University, Xi'an 710072, PR China

Received 27 July 2012; received in revised form 7 August 2012; accepted 7 August 2012
Available online 20 August 2012

Abstract

The carbon-doped Li_2SnO_3/graphene composites for lithium-ion batteries were synthesized by the hydrothermal route. The structure, morphology and electrochemical properties of the composites were detected by means of XRD, SEM, TEM, Raman, TGA and electrochemical measurements. The Li_2SnO_3 nanoparticles are surrounded by graphene sheets (GNS) and amorphous carbon layers. The carbon-doped Li_2SnO_3/graphene materials exhibit good electrochemical performance with high capacity and good cycling stability (736.3 mA h/g after 50 cycles at 60 mA/g).The presence of graphene sheets and carbon layer can alleviate the effects of volume changes, keep the structure stable and increase the conductivity. Conclusively, The C/Li_2SnO_3/GNS composites exhibit better electrochemical properties than GNS/Li_2SnO_3 and Li_2SnO_3.
© 2012 Elsevier Ltd and Techna Group S.r.l. All rights reserved.

Keywords: Carbon-doped Li_2SnO_3/graphene; Hydrothermal route; Lithium-ion batteries; Electrochemical properties

1. Introduction

The lithium-ion battery is considered to be an excellent portable electronic product and electric vehicle power, owing to its small size, and high energy density. In spite of the commercialization of the carbon material, the capacity is still relatively low (372 mA h/g) [1]. Thus, much effort has been made to develop alternative electrode materials which own higher lithium storage capacity. Among the large number of alternative anode materials, tin-based materials have been received researchers' attention, owing to the high theoretical capacity (993 mA h/g) [2]. Tin alloys [3–6] and tin-based oxides [7–9] are considered as anode materials for lithium-ion battery. A tin-based metal salt-Li_2SnO_3, also has a higher theoretical capacity than graphite and it has become the potential anode material [10]. The severe volume expansion of Li_2SnO_3 in an alloy reaction is the most adverse factor that has bad influence on its performance. Doping/coating with buffer materials (such as carbon) is the strategy to relieve the volume changes [11].The carbon layers can not only buffer the volume change, but also enhance the conductivity.

Graphene as a new carbon material has a unique structure, high specific surface area, and specific electronic conduction [12]. The reversible capacity of graphene is 330–~1054 mA h/g, which is based on its unique two-dimensional structure that provides a high specific surface area, and it is also considered that surface functional groups and structural disorder/defects are caused [13]. Lian et al. [14] prepared the high-quality graphene flakes by rapid thermal expansion whose initial reversible capacity is 1264 mA h/g and the reversible capacity is 848 mA h/g after 40 cycles. Graphene is a relatively stable carrier which can be compounded with other anode materials and the accession of graphene can effectively alleviate the serious volume expansion of the anode material in the process of intercalation and deintercalation of lithium; meanwhile that makes it easier to synergize with active materials, which can exhibit higher specific capacity and better cycling performance than the original materials. Zhao prepared SnO_2/graphene material which shows a discharge capacity of 775.3 mA h/g after 50 cycles [15].

*Corresponding author. Tel.: +86 29 88431636.
E-mail addresses: zhaoyang890@163.com (Y. Zhao), yingh@nwpu.edu.cn (Y. Huang).

0272-8842/$ - see front matter © 2012 Elsevier Ltd and Techna Group S.r.l. All rights reserved.
http://dx.doi.org/10.1016/j.ceramint.2012.08.020

In this work, we synthesized C/Li_2SnO_3/graphene by a hydrothermal technique and subsequent calcination. In this way, Li_2SnO_3 nanoparticles were properly wrapped between the graphene sheets and the amorphous carbon coating layers [16]. Then, as-prepared C/Li_2SnO_3/graphene shows the synergistic properties and superior electrochemical performance.

2. Experimental

2.1. Synthesis procedures

2.1.1. Synthesis of Li_2SnO_3/graphene

Graphite oxide was first synthesized with a modified Hummers' method [14,15]. Then, graphene nanosheets (GNS) were deoxidated with the thermal expansion reduction method [17]. After having been synthesized, Li_2SnO_3 then grew onto the graphene sheets in a hydrothermal process. In a typical way, 300 mg graphene nanosheets and 0.5012 g Cetyltrimethyl Ammonium Bromide(CTAB) were dispersed into 100 ml ethanol by ultrasonication, and we labeled the mixture solution A. B solution was prepared by dissolving 7.1783 g of $SnCl_4 \cdot 5H_2O$ into 20 mL of ultrapure water. After mixing the two solutions, we added 5.0162 g LiOH into the mixture slowly. Then the resultant mixture was transferred to a Teflon-lined stainless steel autoclave and kept in an oven at 180 °C for 18 h. Then, the product was separated and washed for several times with ultrapure water and ethanol after the hydrothermal reaction was terminated. After these, the product was dried under vacuum at 60 °C for 12 h to obtain the precursor. Finally, the precursor was sintered at 800 °C for 4 h under argon atmosphere to obtain Li_2SnO_3/graphene composites.

2.1.2. Synthesis of C/Li_2SnO_3/graphene

For the carbon-doped composites, the precursor was dispersed into 100 mL ultrapure water, followed by ultrasonication for 30 min, and then we added 0.3 g glucose into it. The solution was stirred for 1 h. The mixture was then transferred to a Teflon-lined stainless steel autoclave and kept in an oven at 180 °C for 18 h. The product was collected when the autoclave cooled and then washed with ultrapure water. Finally, we got the black precipitate. The black precipitate was dried under vacuum at 60 °C for 12 h, followed by being sintered at 800 °C for 4 h under argon atmosphere to obtain C/Li_2SnO_3/graphene composite.

2.2. Materials characterization

The structures of the prepared samples were characterized by X-ray diffraction analysis (XRD) (Rigaku, model D/max-2500 system at 40 kV and 100 mA of Cu K), the Raman spectra by an inVia Laser-Raman spectrometer (Renishaw Co., England) with 514 nm radiation, the surface morphology study by the model Tecnai F30 G2 (FEI Co., USA) field emission transmission electron microscope (FETEM) and scanning electron microscope (SEM, SuPRA 55, German ZEISS), the thermal analysis by thermal gravimetric analysis (TGA) (Model Q50, TA, USA) under an air atmosphere, with a heating rate of 20 °C/min whose temperature range was from 20 to 800 °C.

Electrochemical performance was evaluated by CR2016-type coin cell with a multi-channel current static system Land (LAND CT200IA). The anode electrodes were prepared by coating slurries containing C/Li_2SnO_3/graphene nanocomposite (65 wt%) with acetylene black (15 wt%) and PVDF(20 wt%) as a binder dissolved in 1-methyl-2-pyrrolidinone(NMP) solution on a copper foil. Li foil was used as counter electrode, polypropylene (PP) film (Celgard 2400) as separator. The electrolyte was a solution of 1 M $LiPF_6$ in a mixture of ethylene (EC), dimethyl carbonate (DMC) and diethyl carbonate (DEC) (1:1:1, v/v/v).

3. Results and discussion

Fig. 1 shows the X-ray diffraction (XRD) patterns of the graphite oxide (a, GO), graphene (b), precursor $Li_2Sn(OH)_6$/GNS (c), Li_2SnO_3/GNS (d), and C/Li_2SnO_3/GNS (e). The diffraction pattern peak is shown at around 10.98° characteristic of GO (a), that of graphene (b) shows a peak at about 26°, which depends on graphite-like (002) reflections. In Fig. 1(c) all diffraction peaks are in good agreement with the standard data for the monoclinic crystal structure

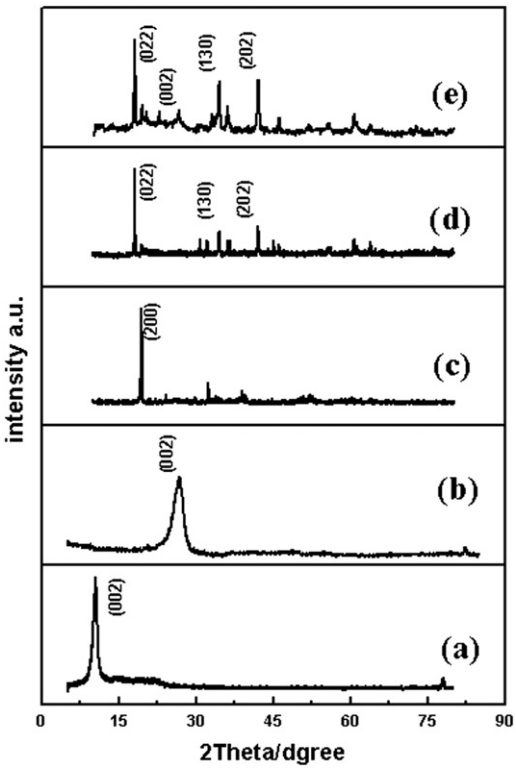

Fig. 1. XRD patterns of graphite oxide (a), graphene (b), precursor $Li_2Sn(OH)_6$/GNS (c), Li_2SnO_3/GNS (d), and C/Li_2SnO_3/GNS (e).

$Li_2Sn(OH)_6$ (PDF#52-0489). The hydrothermal reaction mechanism can be described as follows:

$$SnC1_4 + 4LiOH \rightarrow Sn(OH)_4$$

$$Sn(OH)_4 + 2LiOH \rightarrow Li_2Sn(OH)_6$$

The diffraction patterns of Li_2SnO_3/GNS (Fig. 1(d)) match well with the structure of Li_2SnO_3.The standard data of Li_2SnO_3 monoclinic crystal structure with lattice constants $a=5.301$ Å, $b=9.181$ Å, and $c=10.027$ Å (PDF#31-0761). shows that accession of the graphene will not affect the hydrothermal reaction, and it may provide a nucleus for the crystal growth in the reaction. The C/Li_2SnO_3/graphene (Fig. 1e) also shows a strong pattern of Li_2SnO_3. At the same time, the C peak at 26° is identified. Conclusively, all of the two patterns show broadened diffraction peaks, indicating the formation of fine Li_2SnO_3 crystals.

Fig. 2 presents the Raman spectra of Li_2SnO_3/GNS (c), C/Li_2SnO_3/graphene (d), with the Raman spectrum of GO (a) and GNS (b) shown for comparison. The peak at about 1592 cm^{-1} (G band) is owing to the vibration of sp^2-bonded carbon atoms in a 2-dimensional hexagonal lattice, while the 1334 cm^{-1} peak (D band) can be owing to the defects and disorder in the hexagonal graphitic layers [15,16]. In Fig. 2, it can be identified that the ID/IG of GO is 0.88 and the ID/IG of GNS is 0.92, while the value of ID/IG is 0.77 for GNS/Li_2SnO_3 and the ID/IG of C/Li_2SnO_3/GNS is 1.03. When we pyrolyze GO to form GNS in Ar, the mass of GO will increase with a large number of gases emission, such as CO_2, CO and H_2O. The gases emission results in the carbon atoms and functional groups loss from the surface and the interior, which engender a lot of carbon cavities and increase the disorder degree of GNS. This may explain that the ID/IG of GNS (0.92) is higher than GO (0.88). Obviously, because of the addition of amorphous carbon, the ID/IG of C/Li_2SnO_3/GNS (1.03) is much higher than that of the GNS/Li_2SnO_3 (0.77).

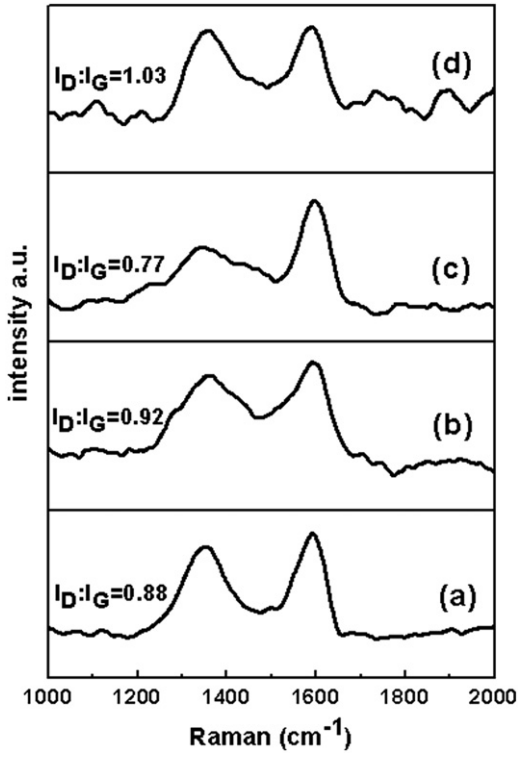

Fig. 2. Raman spectra of GO (a), graphene (b), Li_2SnO_3/GNS (c), and C/Li_2SnO_3/GNS (d).

Fig. 3 shows the analysis of TGA of the two samples that are characterized in air. In Fig. 3, an abrupt weight loss occurs from 200 °C to 500 °C, indicating the oxidation and decomposition of graphene and amorphous carbon occurs in air. The weight loss from 50 °C to 140 °C may be contributed by the evaporation of water. Therefore, the change in weight before and after the oxidation of graphene or carbon can be transformed into the change in amount of graphene and carbon in the materials, respectively. The TGA curves show the mass fraction of graphene in the Li_2SnO_3/GNS is about 18 wt%, the amount of carbon and graphene in the C/Li_2SnO_3/GNS is about 30 wt%. The accession of the amorphous carbon improves the carbon content of the sample.

Scanning electron microscopy (SEM) images (Fig. 4a and b) show that Li_2SnO_3/GNS and C/Li_2SnO_3/GNS have the uniform morphology over large domains. It can be observed from the figures that the two samples possess good electrical conductivity. In all cases, Li_2SnO_3 nanoparticles are distributed on the voile-like graphene sheets.

Fig. 4(c) shows the low-magnification and high-magnification TEM images of the graphene nanosheets. Sheet-like graphene with numerous folds at the edges can be found in these images. In the high-magnification TEM images (Fig. 4d), it can be observed that the thickness of graphene nanosheets is about 3 nm, corresponding to nine layers as pure single-layer graphene flake which has a thickness of 0.34 nm. The TEM images of Li_2SnO_3/GNS (Fig. 4e) clearly illustrate that Li_2SnO_3 nanocrystals

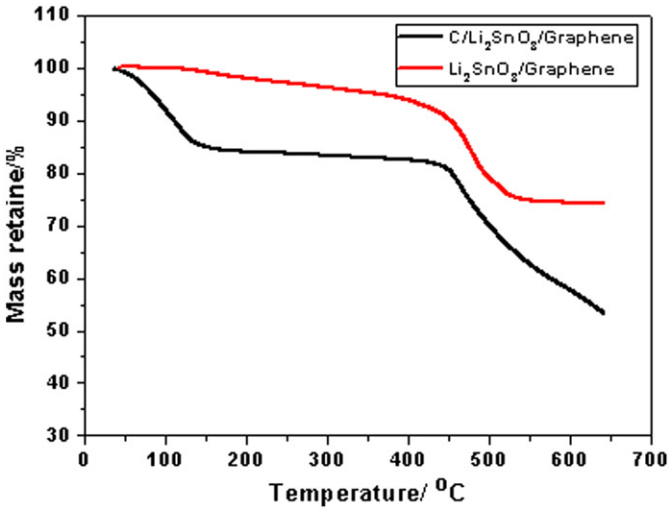

Fig. 3. TGA curves of the Li_2SnO_3/GNS and C/Li_2SnO_3/GNS.

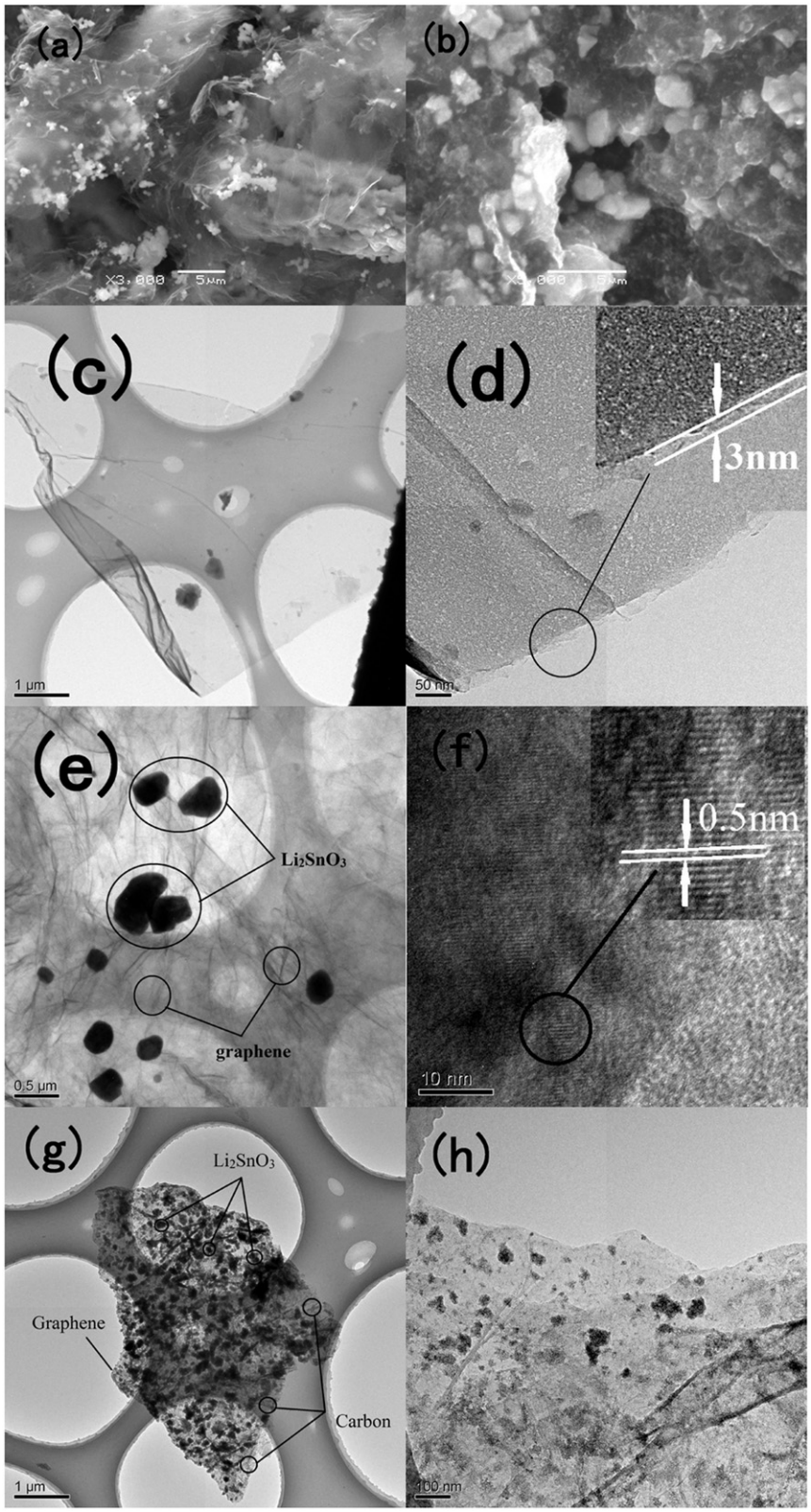

Fig. 4. SEM images of (a) Li_2SnO_3/GNS and (b) C/Li_2SnO_3/GNS; TEM images of graphene (c), Li_2SnO_3/GNS (e) and C/Li_2SnO_3/GNS (g); HRTEM images of graphene (d), Li_2SnO_3/GNS (f) and C/Li_2SnO_3/GNS (h).

are distributed sporadically on the surface of graphene nanosheets. The diameters of the Li_2SnO_3 grains are about 200 nm. In the high-magnification TEM images of Li_2SnO_3/GNS (Fig. 4f), about 0.5 nm spacing of lattice corresponds to the (002) plane of monoclinic Li_2SnO_3, which is in agreement with the XRD analysis.

The structures of the C/Li_2SnO_3/GNS are presented in Fig. 4g and h. Besides sheet-like graphene and Li_2SnO_3 nanoparticles, carbon layer can be found on the edges of the crystal. Therefore, the Li_2SnO_3 nanoparticles are surrounded by the graphene sheets and the amorphous carbon layers, which provide a perfect carbon network structure, electronic transmission channel, stable multi-carrier and can also buffer the volume changes to improve the electrochemical performance as an anode material for lithium ion batteries.

The lithium storage capacity and cyclability of as anode in lithium ion cells are determined via galvanostatic charge/discharge cycling. Fig. 5 shows the charge/discharge profiles of C/Li_2SnO_3/GNS electrode in the first and second cycles, respectively. In the first cycle, the C/Li_2SnO_3/GNS delivers a lithium insertion capacity of 2171.3 mA h/g and a reversible charging capacity of 1060 mA h/g. In the second cycle, the reversibility of the electrode is improved significantly and the irreversible discharge capacity after the first cycle is unlikely/unexpectedly gone away due to severe side reaction with the electrolyte forming Li_2O and solid electrolyte interphase (SEI) film. The reaction between Li_2SnO_3 and Li^+ can be described as [19]

$$Li_2SnO_3 + 4Li \rightarrow 3Li_2O + Sn \quad (1)$$

$$Sn + xLi \leftrightarrow LixSn (x \leq 4.4) \quad (2)$$

To evaluate the rate performance of the C/Li_2SnO_3/GNS composites, the charge/discharge measurements are carried out at various current densities in Fig. 6. At a current density of 60 mA/g (corresponding to about 0.1 C rate), the charge capacity of the composites can remain about 763.3 mA h/g up to 50 cycles, when we increase the current density to 180 mA/g (0.3 C), 300 mA/g (0.5 C) and 600 mA/g (1 C), correspondingly. The composites still can deliver a capacity of 622.7 mA h/g, 569.7 mA h/g and 518.4 mA h/g up to 50 cycles. Despite the large declination capacity of the composites decline largely at high rates, the composites still have an excellent cycling performance, indicating that the GNS and carbon addition is effective. The capacity of the composite at high rates is higher than of Li_2SnO_3.

The galvanostatic charge/discharge cycling results are shown in Fig. 7. The Li_2SnO_3 shows a reversible specific capacity of around 1002.1 mA h/g at a current density of 60 mA/g. However, the capacity drops dramatically to about 263 mA h/g at the 30th cycle. The reversible specific capacity of GNS/Li_2SnO_3 is 983.3 mA h/g. which has gradually attenuated to 576.5 mA h/g after 50 cycles. The C/Li_2SnO_3/GNS shows a good cycle performance and the capacity is 763.3 mA h/g at the 50th cycle. The results indicate that the graphene nanosheets have a beneficial effect on the enhanced stability of the Li_2SnO_3 during the Li alloying/de-alloying process. The volume expansion of Li_2SnO_3 can be buffered by the flexible graphene nanosheets [15]. However, the carbon network structure shows the better modification,

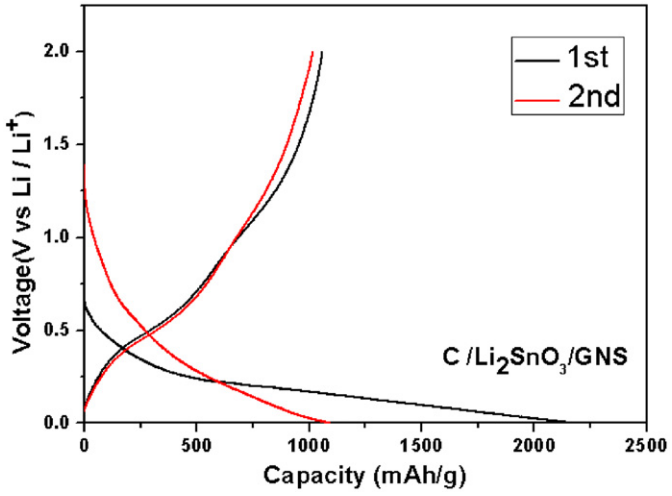

Fig. 5. First and second cycle charge–discharge voltage profiles for C/Li_2SnO_3/GNS at current density of 60 mA/g.

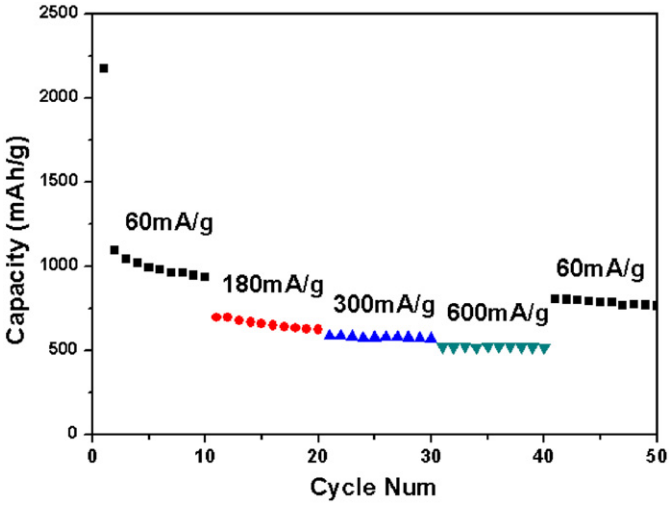

Fig. 6. Cycling performance of the C/Li_2SnO_3/GNS at various charge–discharge current densities.

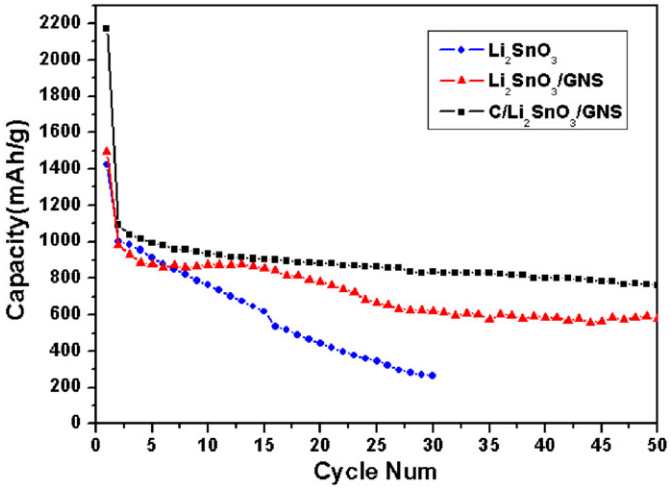

Fig. 7. Cycling performances of Li_2SnO_3, Li_2SnO_3/GNS and C/Li_2SnO_3/GNS at current density of 60 mA/g.

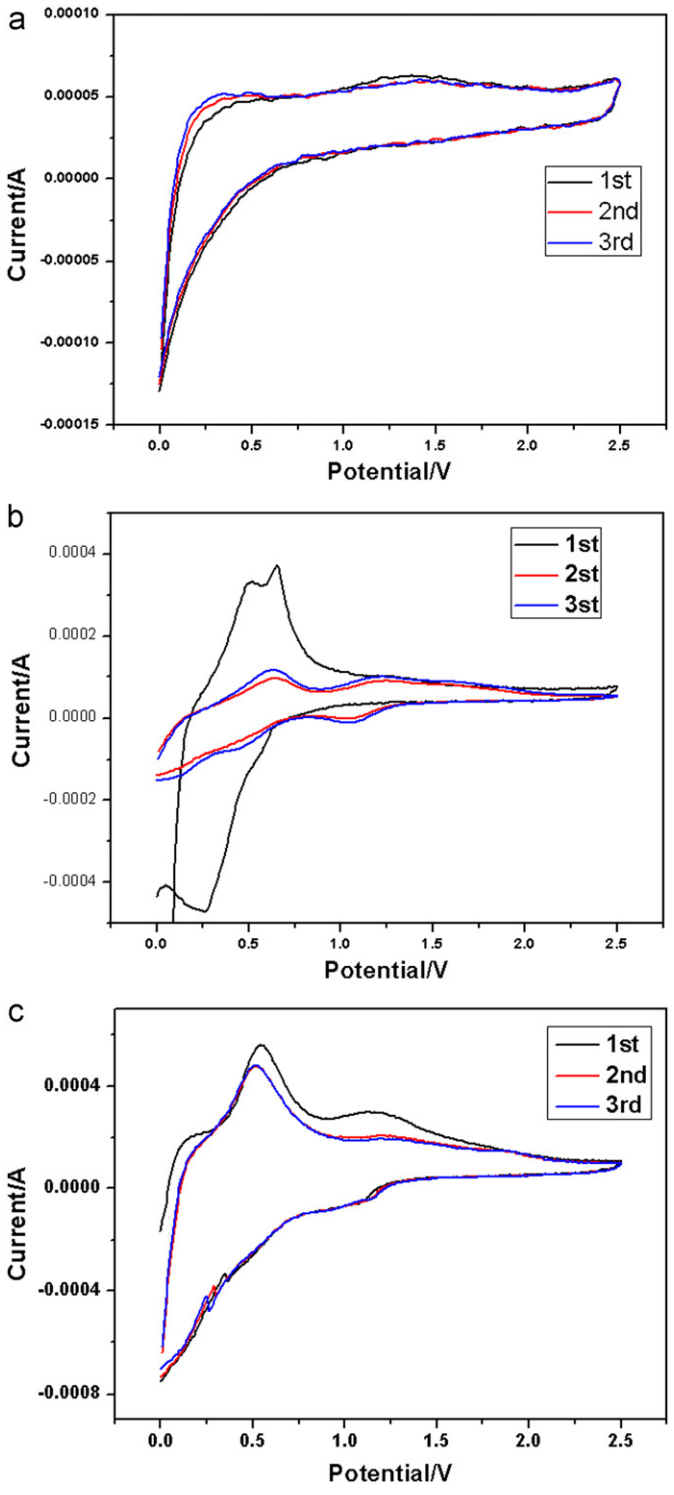

Fig. 8. Cyclic voltammetry of graphene (a), Li_2SnO_3/GNS (b) and C/Li_2SnO_3/GNS (c).

that the volume expansion of Li_2SnO_3 is limited between the graphene sheets and the amorphous carbon layers.

The electrochemical reactivity of the graphene and the composites as anode in lithium-ion battery are evaluated by cyclic voltammetry (CV). Fig. 8 shows the CV curves of graphene, Li_2SnO_3/GNS, and C/Li_2SnO_3/GNS electrodes in the first, second, and third scanning cycles, respectively. Graphene has no evident oxidation/reduction peak, despite a wide voltage range for charge and discharge. Fig. 8(b) shows the CV curve of Li_2SnO_3/GNS. In the first cycle, there is a cathodic peak at 0.25 V, which can be attributed to the formation of the solid electrolyte interphase (SEI) layer. But, this peak disappears in the next cycles. The other obvious reduction peaks are at around 0.5 and 1.2 V, and they can be ascribed to the lithium reaction with Li_2SnO_3 nanoparticles and insertion in graphene nanosheets, respectively. There are three oxidation peaks at 0.15, 0.6, and 1.25 V, respectively. The anodic peak at 0.15 V corresponds to lithium extraction from graphene nanosheet; the oxidation peak at 0.6 V can be assigned to the de-alloying of Li_xSn [18], while the weak oxidation at 1.25 V may be the partly reversible reaction of whole process. The CV measurements clearly elucidate the reversible electrochemical reactions between the lithium ions and the Li_2SnO_3/GNS in lithium-ion battery and the oxidation/reduction peak of C/Li_2SnO_3/GNS (Fig. 8c) similarly with the peak of Li_2SnO_3/GNS. The addition of the amorphous carbon does not affect the CV curve.

Fig. 9 shows the EIS analysis of the electrodes of Li_2SnO_3, Li_2SnO_3/GNS, and C/Li_2SnO_3/GNS at 0.5 V before cycling. The impedance curves consist of one semicircle in the medium frequency region and an inclined line in the low-frequency region. The impedance plots can be fitted by the equivalent circuit diagram. In the equivalent circuit diagram of C/Li_2SnO_3/GNS, Rs stands for the electrolyte resistance (about $1.009 \times 10^{-12}\,\Omega$), Rf stands for the SEI resistance (about 600 Ω), Rct stands for the charge-transfer resistance (about 900 Ω), *W* stands for the Warburg impedance related to the diffusion of lithium ions into the bulk of the electrode materials, CPE1 and CPE2 are two constant phase elements associated with the interfacial resistance and charge-transfer resistance, respectively [19]. The plots also show that the semicircle arc of Li_2SnO_3/GNS is smaller than that of both of those mentioned above, which presents a smaller electrochemical reaction resistance because of the carbon improved electronic contact between the active particles. Conclusively, the electrode conductivity can be greatly increased by the carbon addition [20].

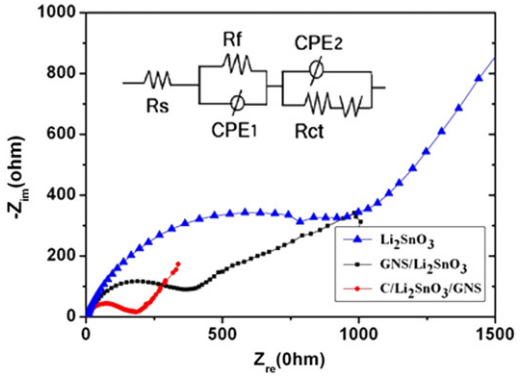

Fig. 9. EIS plots of Li_2SnO_3, Li_2SnO_3/GNS and C/Li_2SnO_3/GNS.

4. Summary

Graphene–Li_2SnO_3 materials were prepared by a hydrothermal technique, and carbon-doped Li_2SnO_3/GNS composites had also been synthesized with the hydrothermal method followed by carbonization. When tested for lithium storage, the C/Li_2SnO_3/GNS composites show significantly improved cycling performance compared to the Li_2SnO_3 and Li_2SnO_3/GNS. A high capacity of 763.3 mA h/g can be retained after 50 cycles at current density of 60 mA/g. When we increase the current density to 600 mA h/g, the reversible capacity of the composite is also retained to 518.4 mA h/g. The graphene sheets and the amorphous carbon layers constitute a perfectly carbon network structure, which is demonstrated to be an effective way to improve the cycling performance of anode materials for lithium ion batteries. Conclusively, the structure can enhance the conductivity, buffer the volume changes and keep the entire composite stable.

References

[1] Y.P. Wu, C. Jiang, C. Wan, R. Holze, Anode materials for lithium ion batteries by oxidative treatment of common natural graphite, Solid State Ionics 156 (2003) 283–290.

[2] Jose L. Tirado, Inorganic materials for the negative electrode of lithium-ion batteries: state-of-the-art and future prospects, Materials Science and Engineering 40 (2003) 103–136.

[3] J.T. Lia, J. Swiatowsk, A. Seyeux, L. Huang, V. Maurice, S.G. Sun, et al., XPS and ToF–SIMS study of Sn–Co alloy thin films as anode for lithium ion battery, Journal of Power Sources 195 (2010) 8251–8257.

[4] Y.X. Wang, L. Huang, Y.Q. Chang, F.S. Ke, J.T. Li, S.G. Sun, Fabrication and electrochemical properties of the Sn–Ni–P alloy rods array electrode for lithium-ion batteries, Electrochemistry Communications 12 (2010) 1226–1229.

[5] R. Yang, J. Huang, W. Zhao, W.Z. Lai, X.Z. Zhang, J. Zheng, Bubble assisted synthesis of Sn–Sb–Cu alloy hollow nanostructures and their improved lithium storage properties, Journal of Power Sources 195 (2010) 6811–6816.

[6] X.L. Wang, W.Q. Han, J.J. Chen, J. Graetz, Single-crystal intermetallic M–Sn (M=Fe, Cu, Co, Ni) nanospheres as negative electrodes for lithium-ion batteries, Applied Materials and Interfaces 2 (2010) 1548–1551.

[7] L.F. Cui, J. Shen, F.Y. Cheng, Z.L. Tao, J. Chen, SnO_2 nanoparticles @polypyrrole nanowires composite as anode materials for rechargeable lithium-ion batteries, Journal of Power Sources 196 (2011) 2195–2201.

[8] W.S. Yuan, Y.W. Tian, G.Q. Liu, Synthesis and electrochemical properties of pure phase Zn_2SnO_4 and composite Zn_2SnO_4/C, Journal of Alloys and Compounds 506 (2010) 683–687.

[9] X.M. Yin, C.C. Li, M. Zhang, Q.Y. Hao, S. Liu, L.B. Chen, T.H. Wang, One-step synthesis of hierarchical SnO_2 hollow nanostructures via self-assembly for high power lithium ion batteries, Journal of Physical Chemistry C 114 (2010) 8084–8088.

[10] D.W. Zhang, S.Q. Zhang, Y. Jin, T.H. Yi, S. Xie, C.H. Chen, Li_2SnO_3 derived secondary Li–Sn alloy electrode for lithium-ion batteries, Journal of Alloys and Compounds 415 (2006) 229–233.

[11] Q.F. Wang, Y. Huang, J. Miao, Y. Zhao, Y. Wang, Synthesis and properties of carbon-doped Li_2SnO_3 nanocomposite as cathode material for lithium-ion batteries, Materials Letters 71 (2012) 66–69.

[12] A.K. Geim, Graphene: status and prospects, Science 324 (2009) 1530–1534.

[13] D.Y. Pan, S. Wang, B. Zhao, Li storage properties of disordered graphene nanosheets, Chemistry of Materials 21 (2009) 3136–3142.

[14] P.C. Lian, X.F. Zhu, S.Z. Liang, Z. Li, W.S. Yang, H.H. Wang, High reversible capacity of SnO_2/graphene nanocomposite as an anode material for lithium-ion batteries, Electrochimica Acta 55 (2010) 3909–3914.

[15] B. Zhao, G.H. Zhang, J.S. Song, Y. Jiang, H. Zhuang, P. Liu, T. Fang, Bivalent tin ion assisted reduction for preparing graphene/SnO_2 composite with good cyclic performance and lithium storage capacity, Electrochimica Acta 56 (2011) 7340–7346.

[16] C.F. Zhang, X. Peng, Z.P. Guo, C.B. Cai, Z.X. Chen, D. Wexler, Carbon-coated SnO_2/graphene nanosheets as highly reversible anode materials for lithium ion batteries, Carbon 50 (2012) 1897–1903.

[17] L.J. Wan, Z.Y. Ren, H. Wang, G. Wang, X. Tong, S.H. Gao, Graphene nanosheets based on controlled exfoliation process for enhanced lithium storage in lithium-ion battery, Diamond and Related Materials 20 (2011) 756–761.

[18] J. Yao, X.P. Shen, B. Wang, H.K. Liu, G.X. Wang, In situ chemical synthesis of SnO_2–graphene nanocomposite as anode materials for lithium-ion batteries, Electrochemistry Communications 11 (2009) 1849–1852.

[19] Q.F. Wang, Y. Huang, J. Miao, Y. Wang, Y. Zhao, Hydrothermal derived Li_2SnO_3/C composite as negative electrode materials for lithium-ion batteries, Applied Surface Science 258 (2012) 6923–6929.

[20] L.S. Zhang, L.Y. Jiang, H.J. Yan, W.D. Wang, W. Wang, W.G. Song, Mono dispersed SnO_2 nanoparticles on both sides of single layer graphene sheets as anode materials in Li-ion batteries, Journal of Materials Chemistry 20 (2010) 5462–5467.